Targeting oncogenic serine/threonine-protein kinase BRAF in cancer cells inhibits angiogenesis and abrogates hypoxia

Alessia Bottos[a,b,1,2], Miriam Martini[b,c,1,3], Federica Di Nicolantonio[c,d], Valentina Comunanza[a,b], Federica Maione[b,e], Alberto Minassi[f], Giovanni Appendino[f], Federico Bussolino[a,b,4,5], and Alberto Bardelli[b,c,d,4,5]

[a]Laboratory of Vascular Oncology, Institute for Cancer Research and Treatment, 10060 Turin, Italy; [b]Department of Oncological Sciences, University of Torino, 10060 Turin, Italy; [c]Laboratory of Molecular Genetics, Institute for Cancer Research and Treatment, 10060 Turin, Italy; [d]Fondazione Italiana per la Ricerca sul Cancro Institute of Molecular Oncology, 20139 Milan, Italy; [e]Laboratory of Transgenic Mouse Models, Institute for Cancer Research and Treatment, 10060 Turin, Italy; and [f]Dipartimento di Scienze Chimiche, Alimentari, Farmaceutiche e Farmacologiche, Universitá del Piemonte Orientale, 28100, Novara, Italy

Edited* by Napoleone Ferrara, Genentech, South San Francisco, CA, and approved November 18, 2011 (received for review April 1, 2011)

Carcinomas are comprised of transformed epithelial cells that are supported in their growth by a dedicated neovasculature. How the genetic milieu of the epithelial compartment influences tumor angiogenesis is largely unexplored. Drugs targeted to mutant cancer genes may act not only on tumor cells but also, directly or indirectly, on the surrounding stroma. We investigated the role of the $BRAF^{V600E}$ oncogene in tumor/vessel crosstalk and analyzed the effect of the BRAF inhibitor PLX4720 on tumor angiogenesis. Knock-in of the $BRAF^{V600E}$ allele into the genome of human epithelial cells triggered their angiogenic response. In cancer cells harboring oncogenic BRAF, the inhibitor PLX4720 switches off the ERK pathway and inhibits the expression of proangiogenic molecules. In tumor xenografts harboring the $BRAF^{V600E}$, PLX4720 extensively modifies the vascular network causing abrogation of hypoxia. Overall, our results provide a functional link between oncogenic BRAF and angiogenesis. Furthermore, they indicate how the tumor vasculature can be "indirectly" besieged through targeting of a genetic lesion to which the cancer cells are addicted.

targeted therapy | tumor suppressor gene | personalized medicine

Angiogenesis is a pivotal process for the growth, maintenance, and spread of the majority of solid tumors. In the early steps of carcinogenesis, tumor cells require oxygen and nutrients, which are supplied by newly formed vessels. During later phases of cancer progression, blood vessels provide one of the most important routes for tumor escape and metastasization (1, 2). Notably, the structure of the vascular network dramatically alters tumor features. Tumor vessels are disorganized, with perfusion defects resulting in metabolic changes, hypoxia, and increase in interstitial pressure (3). At the clinical level, these features are associated with a more aggressive phenotype and a reduction of drug delivery to the tumor mass (4, 5).

The angiogenic process is triggered and controlled by the cancer cells, which carry genetic lesions that are causally associated with the neoplastic process. Understanding how individual genetic lesions in oncogenes and tumor suppressor genes affect directly or indirectly the angiogenic process is a fundamental question that has been largely unexplored. It has been suggested that alterations in oncogenes involved in the intracellular MAPK signaling cascade play a central role in regulating tumor angiogenesis (6). For example, KRAS activating mutations are thought to sustain the chaotic tumor vasculature by up-regulating the transcription of angiogenic inducers, including VEGF-A and IL-8 (7–9). BRAF binds to and is the main downstream effector of KRAS. Whether and to what extent genetic alterations affect BRAF-regulated angiogenesis is presently unclear. The most common BRAF mutation is a valine-to-glutamate transition (V600E), which results in constitutive activation of the kinase activity. $BRAF^{V600E}$ is causally involved in the onset and progression of several cancers, including melanoma, papillary thyroid, colorectal, and ovarian tumors (10–12), and is often associated with a particularly poor prognosis (13–17).

In addition to activation of aberrant cell proliferation, $BRAF^{V600E}$ modulates tumor–stroma interaction and supports cancer invasiveness by influencing the expression of metalloproteinases and cytokines (IL-6 and IL-10) involved in tumor-immune escape (18, 19). Furthermore, $BRAF^{V600E}$ affects tumor environment by enhancing the expression of HIF1α (20–22), VEGF-A and IL-8 (23–25) and inhibiting the angiogenic blocker thrombospondin 1 (26).

Specific and selective BRAF kinase inhibitors, such as PLX4032/PLX4720, have recently shown remarkable clinical success in patients with melanoma carrying the $BRAF^{V600E}$ mutation (27–29).

Considering the putative role of mutant BRAF in modulating cancer cell function and microenvironment, we hypothesized that the efficacy of PLX4720 could result from targeting the epithelial and the stromal tumor compartments. In this work, we assessed the contribution of $BRAF^{V600E}$ oncogene in promoting angiogenesis, and investigated whether the BRAF inhibitor PLX4720 affects tumor angiogenesis and hypoxia.

Results

$BRAF^{V600E}$ Drives Angiogenesis in Chicken Chorioallantoic Membrane. To study the specific influence of $BRAF^{V600E}$ on angiogenesis, we used an isogenic model in which $BRAF^{V600E}$ was knocked-in through homologous recombination into the genome of the nontumorigenic human mammary epithelial cell line (hTERT-HME1) (30). As a result, the mutant allele is expressed under its endogenous promoter at levels comparable to wild type (WT) thus overcoming the experimental drawbacks associated with plasmid-driven ectopic overexpression.

Author contributions: A. Bottos, F.D.N., F.B., and A. Bardelli designed research; A. Bottos, M.M., F.D.N., V.C., and F.M. performed research; A.M. and G.A. contributed new reagents/analytic tools; A. Bottos, M.M., F.D.N., V.C., F.M., F.B., and A. Bardelli analyzed data; and A. Bottos, F.D.N., F.B., and A. Bardelli wrote the paper.

Conflict of interest statement: A. Bardelli owns stock in, and has received consultancy fees from, Horizon Discovery.

*This Direct Submission article had a prearranged editor.

[1]A. Bottos and M.M. contributed equally to this work.

[2]Present address: Friedrich Miescher Institute for Biomedical Research, CH-4058 Basel, Switzerland.

[3]Present address: Department of Genetics, Biology and Biochemistry, Molecular Biotechnology Center, 10100 Turin, Italy.

[4]F.B. and A. Bardelli contributed equally to this work.

[5]To whom correspondence may be addressed. E-mail: federico.bussolino@ircc.it or alberto.bardelli@ircc.it.

See Author Summary on page 1836.

This article contains supporting information online at www.pnas.org/lookup/suppl/doi:10.1073/pnas.1105026109/-/DCSupplemental.

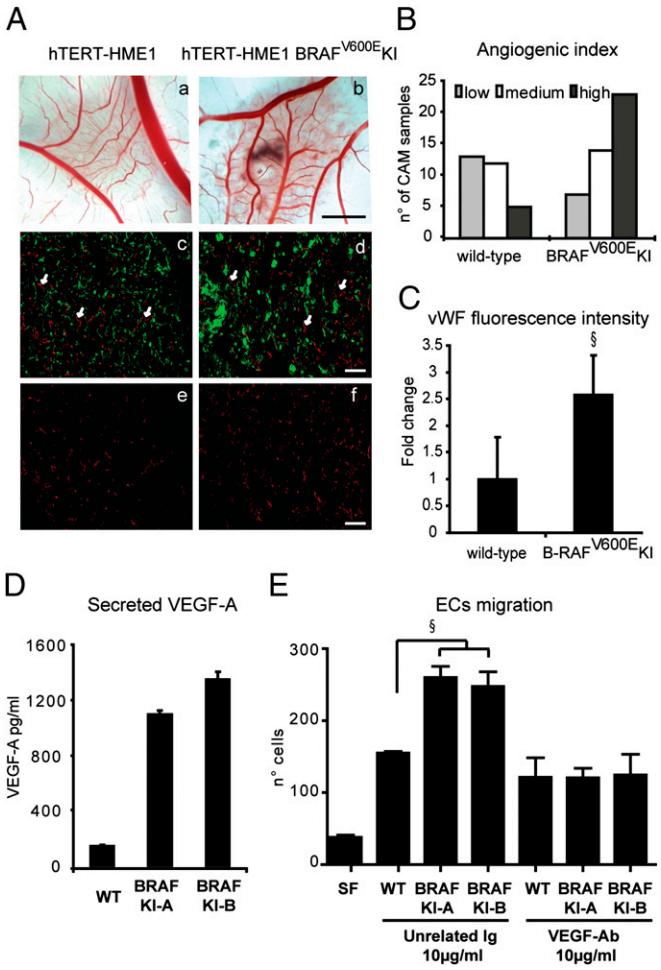

Fig. 1. KI of the BRAFV600E allele in hTERT-HME1 cells enhances angiogenesis in CAM assay and increases VEGF-mediated migration of ECs. (*A*) Representative images of hTERT-HME1 cells plated on the CAM (*a* and *b*). (Scale bar: 1 mm.) Immunofluorescence analysis of hTERT-HME1 cells plated on the CAM. Human epithelial cells were stained with the HLA marker (green) whereas blood vessels were labeled with the vWF, which is specific for ECs (red) (*c–f*). Arrows indicate blood vessels. (Scale bar: 100 μm.) (*B*) Qualitative assessment of angiogenesis (angiogenic index) in the CAM assay (*Materials and Methods*). Bars represent the number of CAM samples that exhibit low, medium, or high angiogenesis in parental or BRAF^{V600E} mutant cells. Measurements were performed by two observers in blinded fashion. (*C*) Quantitative analysis of vWF intensity fluorescence mean in hTERT-HME1 plugs. Data are expressed as fold change mean ± SEM ($^{§}P < 0.05$, Student *t* test; WT hTERT-HME1, $n = 6$; BRAF^{V600E} KI hTERT-HME1, $n = 9$ samples). (*D*) Quantification of secreted VEGF-A in hTERT-HME1 cells by ELISA. Data are expressed as mean ± SD of a technical replicate and are representative of three independent experiments. (*E*) Migration of human ECs is enhanced by the supernatant of hTERT-HME1 BRAF^{V600E} KI cells compared with the WT counterpart. Two different clones of BRAF^{V600E} KI were analyzed (KI-A and KI-B). SF, serum free medium. VEGF blocking antibody (VEGF-Ab), but not unrelated Ig, abolished BRAF^{V600E} -induced cell migration. Bars represent the mean ± SEM of the number of migrated cells of three samples ($^{§}P < 0.05$, Student *t* test). The representative of three independent experiments is shown.

We used the chicken chorioallantoic membrane (CAM) assay to assess whether BRAF^{V600E} could modulate angiogenesis. Compared with WT, BRAF^{V600E} cells growing on CAM led to a disorganized vasculature with several hemorrhagic areas as measured by an arbitrary "angiogenic index" (Fig. 1 *A*, *a* and *b*, and *B*). The quantification of chicken endothelium within the epithelial plugs revealed that BRAF^{V600E} increased the recruitment of endothelial cells (ECs) (Fig. 1 *A*, *c–f*, and *C*).

We next compared the transcriptional profile of genes involved in angiogenesis and inflammation between BRAF^{V600E} and parental hTERT-HME1 cells. To avoid clonal variability, two independent BRAF^{V600E} KI clones were evaluated. The transcription analysis was performed in standard culture conditions (on plastic) and on CAM. This comprehensive approach revealed that oncogenic BRAF^{V600E} enhanced the expression of several proangiogenic and proinflammatory molecules, including VEGF-A and C, TGF-α, and chemokines, such as CXCL1-2–3, IL1β, and IL8 (Fig. S1 shows a list of differentially expressed genes). Importantly, results from cells plated on CAM mirrored those obtained in vitro, indicating that the chicken embryo microenvironment does not influence the transcriptional landscape of the xenografted cells.

The finding that oncogenic BRAF^{V600E} triggers up-regulation of factors known to modulate angiogenesis led us to hypothesize that the occurrence of this mutation in epithelial cells might affect the endothelium. Among the factors that were pinpointed by the transcriptional profile, we focused on VEGF-A because this molecule is a well known master switch of the angiogenic program. BRAF^{V600E} KI cells released higher amounts of VEGF-A in the supernatant that enhanced EC migration compared with the WT counterpart (Fig. 1 *D* and *E*). The chemotactic effect of oncogenic BRAF on the ECs was abrogated by an anti-VEGF blocking antibody, but not by an unrelated Ig (Fig. 1*E*). This observation supports the pivotal role of VEGF-A in BRAF^{V600E} -driven angiogenesis.

PLX4720 Exerts Cytostatic and Antiangiogenic Activities in Tumor Harboring BRAF^{V600E}. We next assessed whether the results obtained by using the non-transformed isogenic cells might hold true in cancer cells carrying the BRAF^{V600E} allele. Cell lines of colorectal cancer (COLO205) and melanoma (SK-MEL-28) origin were selected because these tumor types frequently harbor mutations in the BRAF gene (10). As expected, in vitro treatment with the specific BRAF^{V600E} inhibitor PLX4720 resulted in cell growth inhibition and ERK inactivation in both cell lines, whereas AKT phosphorylation was not affected (Fig. 2 *A* and *B*). Colorectal cancer cells carrying WT BRAF (DiFi) were used as control and proved insensitive to PLX4720 treatment (Fig. 2 *A* and *B*).

We next measured the effect of PLX4720 in vivo by growing COLO205 and SK-MEL-28 subcutaneously in immunocompromised mice. PLX4720 induced a prolonged cytostatic effect in both xenograft models (Fig. 2 *C* and *D*, *a* and *b*). Importantly, PLX4720-treated tumors did not show evident shrinkage and, despite an initial regression in SK-MEL-28, at the end of the experiments, tumor size was stabilized but not reduced. This was further supported by the analysis of proliferation and apoptosis assessed through Ki-67 staining and activation of caspase 3, respectively. We found that PLX4720 markedly inhibited tumor cell proliferation, whereas it was ineffective in inducing apoptosis (Fig. 2 *D*, *c–f*, *E*, and *F*).

We then investigated the impact of PLX4720 on tumor angiogenesis in vivo. As differences in the tumor vasculature might be influenced by cell proliferation and/or tumor size, we introduced a third control group that involved samples obtained when treatment was started. These samples (hereafter referred to as "start point") were carefully chosen to have approximately the same volume of PLX4720-treated tumors. The comparative analysis of the three groups allowed us to investigate the effect of PLX4720 on tumor vasculature. As shown in Fig. 3*A*, PLX4720 induced profound changes in vascular architecture in COLO205 and SK-MEL-28 tumors. In the absence of treatment, the vascularized area in COLO205 tumors did not change throughout the experiment. Conversely, the area occupied by vessels increased in PLX4720-treated samples compared with the vehicle and start-point samples (Fig. 3*B*). This phenotype is likely the consequence of morphological changes in vascular structure.

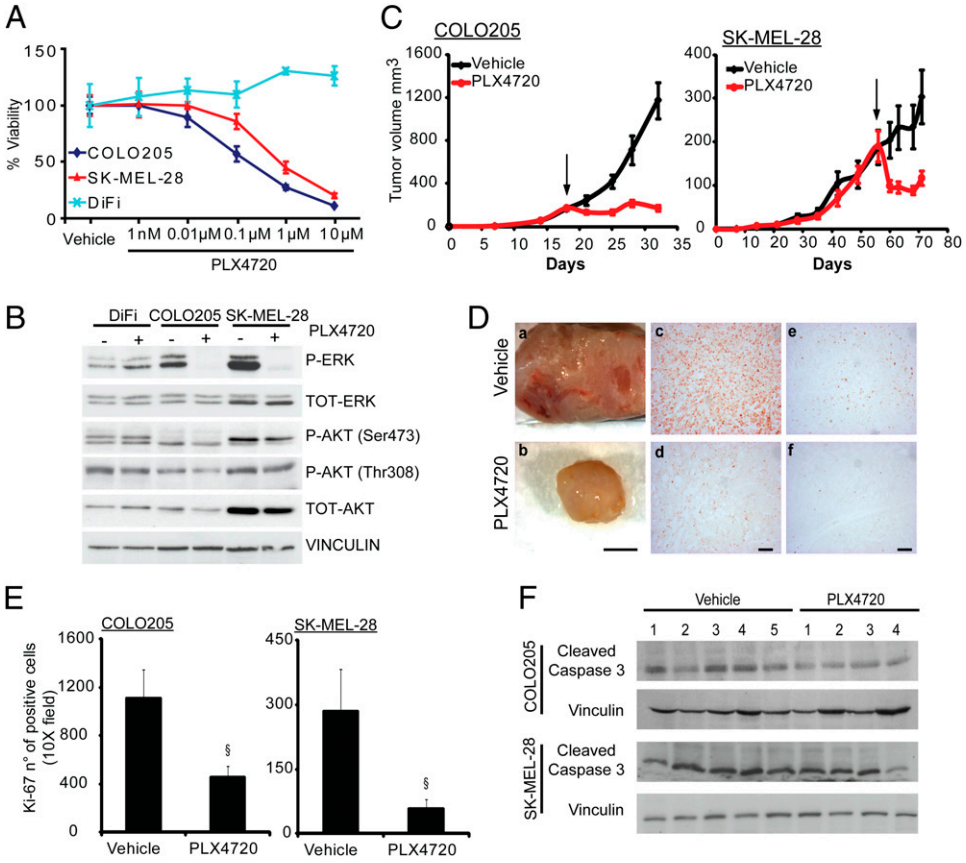

Fig. 2. PLX4720 inhibits proliferation and turns off MAPK signaling in tumor cells carrying $BRAF^{V600E}$. (*A*) Proliferation of COLO205 and SK-MEL-28, harboring $BRAF^{V600E}$, and BRAF WT DiFi cells, was assessed with increased PLX4720 concentration. Data are expressed as percentage of viability compared with vehicle by the ATP assay. Mean ± SD of two independent experiments performed in quadruplicate is shown. (*B*) Biochemical analysis of phospho-ERK and phospho-AKT (Ser473 and Thr308) in COLO205, SK-MEL-28, and DiFi cells. Protein loading was normalized by vinculin. Starved cells were stimulated for 30 min with 2.5% FBS plus 1 μM PLX4720 or vehicle. (*C*) Tumor growth curve of COLO205 and SK-MEL-28 xenografts. COLO205 and SK-MEL-28 xenografts were treated with PLX4720 60 mg/kg or vehicle for 2 wk after tumor volume reached an average of 150 to 200 mm^3. Arrows indicate the time point at which treatment was started. Data are presented as mean tumor volume ± SEM. (*D*) Representative images of COLO205 tumors (*a* and *b*). (Scale bar: 4 mm.) Representative images of Ki-67 staining in COLO205 (*c* and *d*) and SK-MEL-28 (*e* and *f*) xenografts. (Scale bar: 100 μm.) (*E*) Quantification of proliferating cells by Ki-67 staining in COLO205 and SK-MEL-28 xenografts. Bars show the mean of positive cells per 10× field ± SD ($^{§}P < 0.0001$, Student *t* test). For COLO205, vehicle, $n = 4$ mice; PLX4720, $n = 6$ mice; for SK-MEL-28, vehicle, $n = 4$ mice; PLX4720, $n = 5$ mice. (*F*) Biochemical analysis of cleaved caspase 3 in protein extract of COLO205 and SK-MEL-28 xenografts. Protein loading was normalized by vinculin. At least four independent samples were evaluated.

Indeed, blood vessels were enlarged and chaotic in control tumors and thinner with an organized architecture in PLX4720-treated samples (Fig. 3*A*, *a–c*). The average blood vessel diameter decreased from 33 μm or 31 μm in start point and vehicle groups, respectively, to 19 μm in treated samples (Fig. 3*C*). Surprisingly, despite these evident morphological differences, the blood vessel coverage by pericytes was unaffected by PLX4720 treatment (Fig. S2).

In SK-MEL-28 xenografts, the vascularized area increased in vehicle-treated tumors whereas PLX4720 reduced the area occupied by vessels (Fig. 3*B*). Similar to what was observed in COLO205, PLX4720 treatment of SK-MEL-28 tumors increased the vascular surface area compared with start-point tumor. Furthermore, the morphology of the vascular network in SK-MEL-28 was markedly modified and the blood vessel average diameter was reduced from 14 μm compared with 23 μm and 22 μm in start-point and vehicle groups, respectively (Fig. 3 *A*, *d–f*, and *C*).

PLX4720 Abrogates Hypoxia in $BRAF^{V600E}$ Tumors. The aberrant morphology of blood vessels was strongly suggestive of altered functionality of the microvasculature. We confirmed this hypothesis by the analysis of tumor perfusion before and after PLX4720 treatment of COLO205 tumors. Tissue perfusion by blood vessels was strongly increased in PLX4720-treated tumors compared with vehicle or start-point groups, indicating an improved functionality of microvasculature (Fig. 3*D*). Blood perfusion correlates with improved tissue oxygenation, which causes deep changes in the overall features of tumor parenchyma (3).

We therefore studied the effect of PLX4720 on intratumoral hypoxia in COLO205 and SK-MEL-28 xenografts and found that PLX4720 prominently abolished hypoxia in treated tumors compared with vehicle or start-point tumors (Fig. 4 *A*, *a–c* and *g–i*, and *B*). Moreover, analysis of tumor tissues revealed that the modification of vascular structure by PLX4720 was linked to reduced necrotic area in COLO205 and SK-MEL-28 xenografts (Fig. 4 *A d–f* and *j–l*, and *C*). These results indicate that the effect on hypoxia is independent from tumor growth and has implications for the therapeutic activity of PLX4720.

Importantly, targeting of angiogenesis by BRAF inhibition showed significant differences with respect to classical "VEGF directed" antiangiogenic therapy. Treatment of COLO205 tumors with the VEGF-blocking antibody bevacizumab resulted in stabilization of tumor growth and strongly reduced microvascular density (Fig. 5 *A*, *B*, *g* and *h*, and *C*). Concomitantly, tissue perfusion was impaired, and this led to persistent hypoxia and necrosis (Fig. 5 *B* and *D–F*). The comparison between the two

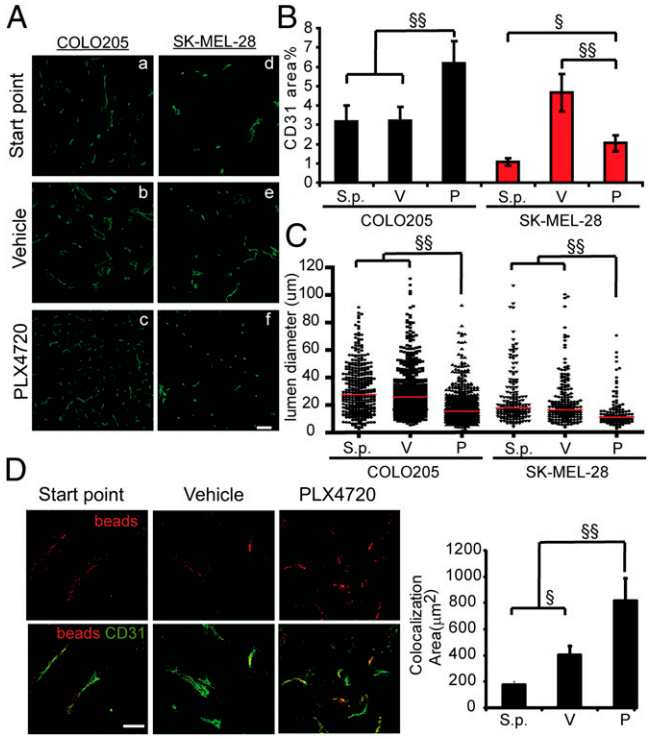

Fig. 3. PLX4720 treatment stabilizes blood vessels in COLO205 and SK-MEL-28 xenograft models. (*A*) Representative images of immunofluorescence analysis with the CD31 endothelial marker (green) in COLO205 (*a–c*) and SK-MEL-28 (*d–f*) tumors. (Scale bar: 100 μm.) (*B*) Percentage of surface area occupied by vessels quantified by CD31 staining. Bars show mean ± SEM. ($^{§§}P < 0.001$ and $^{§}P < 0.01$, Student *t* test). For COLO205, start point, $n = 8$ mice; vehicle, $n = 9$ mice; PLX4720, $n = 14$ mice; for SK-MEL-28, start point, $n = 6$ mice; vehicle, $n = 5$ mice; PLX4720, $n = 5$ mice. (*C*) Quantification of blood vessel lumen diameter. Red bars represent the median for each group ($^{§§}P < 0.0001$, Student *t* test). Dots indicate the individual vessels measured for the indicated cell lines. (*D*) Representative images of colocalization analysis between perfused beads (red) and CD31 (green) in COLO205. (Scale bar: 50 μm.) Quantification is shown as mean ± SEM of colocalization area (in μm^2; $^{§§}P < 0.01$ and $^{§}P < 0.05$, Student *t* test). COLO205, start point, $n = 39$ blood vessels; vehicle, $n = 30$ blood vessels; PLX4720, $n = 35$ blood vessels. S.p., start point; V, vehicle; P, PLX4720.

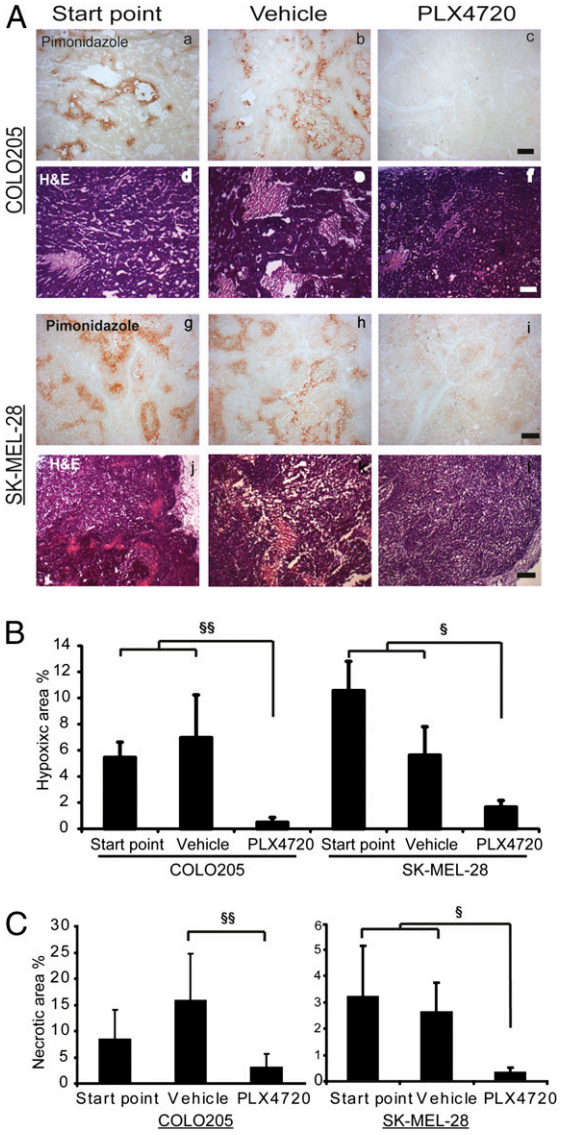

Fig. 4. PLX4720 treatment abolishes tumor hypoxia and decreases necrosis in COLO205 and SK-MEL-28 xenograft models. Histological analysis of COLO205 and SK-MEL-28 xenografts before and after PLX4720 treatment. (*A*) Representative images of pimonidazole and H&E staining in COLO205 (*a–c* and *d–f*) and SK-MEL-28 (*g–i* and *j–l*) tumors. (Scale bar: 100 μm.) (*B*) Quantification of the hypoxic area (percentage) by pimonidazole staining. Bars show mean ± SEM ($^{§§}P < 0.005$ and $^{§}P < 0.05$, Student *t* test). For COLO205, start point, $n = 7$ mice; vehicle, $n = 8$ mice; PLX4720, $n = 8$ mice; for SK-MEL-28, start point, $n = 6$ mice; vehicle, $n = 5$ mice; PLX4720, $n = 5$ mice. (*C*) Quantification of necrotic area after H&E staining in COLO205 and SK-MEL-28 xenografts. Bars represent the percentage mean area ± SEM ($^{§§}P < 0.01$ and $^{§}P < 0.05$, Student *t* test). For COLO205, start point, $n = 8$ mice; vehicle, $n = 9$ mice; PLX4720, $n = 14$ mice; for SK-MEL-28, start point, $n = 6$ mice; vehicle, $n = 5$ mice; PLX4720, $n = 5$ mice.

approaches suggests that antiangiogenic therapy based on inhibition of oncogenes in the epithelial compartment has a greater chance to positively affect the vascular network compared with blockade of the VEGF pathway.

PLX4720 Down-Regulates Expression and Secretion of Proangiogenic Factors in BRAF Mutant Cancer Cells. To further assess whether the antiangiogenic effect of PLX4720 was direct (on the tumor vasculature) or indirect (via epithelial cells), we investigated if PLX4720 affected ECs in vitro. We found that proliferation and migration of ECs were unaffected by drug treatment (Fig. S3), thus ruling out a possible direct effect of BRAF inhibition on the endothelial compartment. We next considered if PLX4720 was capable of modulating the production of angiogenic molecules by cancer cells, which in turn might influence the tumor environment. To assess this, we analyzed the effect of BRAF inhibition on the expression of angiogenic factors in colorectal and melanoma cells carrying mutant BRAF. We found that, upon PLX4720 treatment, multiple mediators of angiogenesis (e.g., CXCL1-2–3, IL-1β, and IL-8 and VEGF-A) were down-regulated in COLO205 and SK-MEL-28. On the contrary, the same genes were not modulated in the BRAF WT DiFi colorectal cancer cells (Fig. 6 *A* and *B*). Additionally, the effect of PLX4720 on VEGF production was not modified by hypoxia, an experimental condition that mimics tumors environment (Fig. 6*B*). Oncogenic BRAF is a key player in the activation of the MAPK-ERK signaling cascade. We therefore reasoned that the control of VEGF expression by PLX4720 might be caused by the inhibition of MAPK signaling. Treatment with the MEK inhibitor AZD6244 decreased VEGF secretion, thus suggesting that MAPK signaling pathway is essential for VEGF expression (Fig. 6*B*). ERK has been previously shown to influence protein translation through the control of the phosphorylation status of

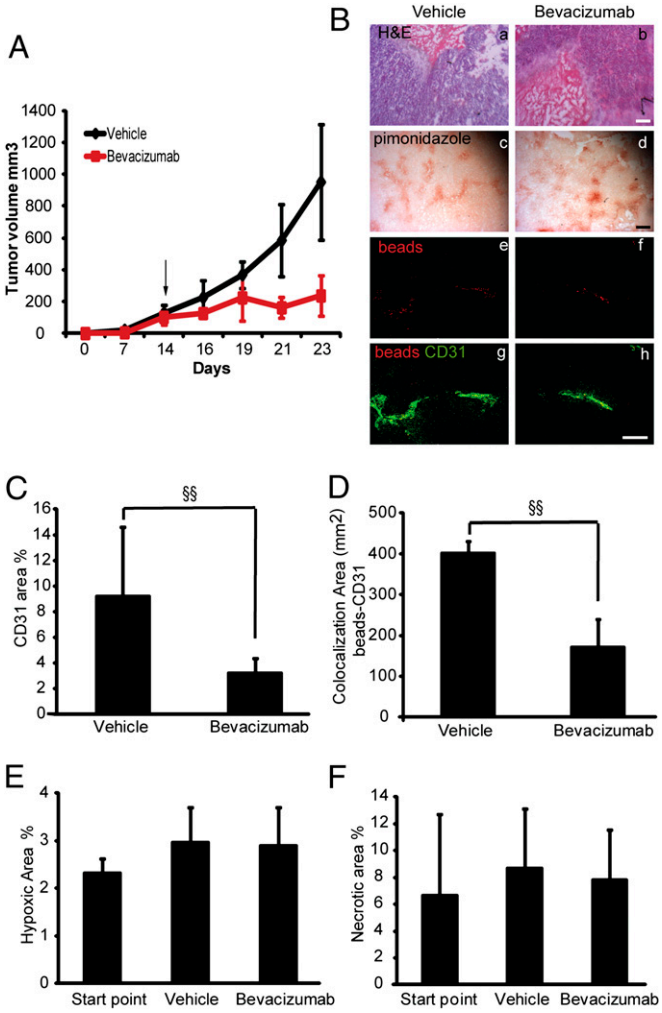

Fig. 5. Effect of bevacizumab on tumor growth and vasculature. COLO205 xenografts were treated with bevacizumab 10 mg/kg or vehicle for 2 wk after tumor volume reached an average of 150 to 200 mm^3. (*A*) Tumor growth curve of COLO205; arrow indicates time point at which treatments were started. Data are presented as mean tumor volume ± SEM of five mice. (*B*) Representative images of H&E (*a* and *b*) and pimonidazole staining (*c* and *d*) in COLO205. (Scale bar: 100 μm.) Colocalization analysis between perfused beads (red) and CD31 (green) in COLO205 (*e*–*h*). (Scale bar: 50 μm.) (*C*) Percentage of surface area occupied by vessels quantified by CD31 staining. Bars show mean ± SEM ($^{§§}P < 0.01$, Student *t* test). Vehicle, $n = 5$ mice; bevacizumab, $n = 6$ mice. (*D*) Analysis of colocalization area between perfused beads and CD31. Quantification is shown as mean ± SEM of colocalization area (in μm^2; $^{§§}P < 0.01$). Vehicle, $n = 35$ blood vessels; bevacizumab, $n = 15$ blood vessels. (*E*) Quantification of the percentage hypoxic area by pimonidazole staining. Bars show mean ± SEM. Start point, $n = 4$ mice; vehicle, $n = 5$ mice; bevacizumab, $n = 6$ mice. (*F*) Quantification of necrotic area by H&E staining. Bars represent the percentage mean area ± SEM. Start point, $n = 4$ mice; vehicle, $n = 5$ mice; bevacizumab, $n = 6$ mice.

p90RSK1, 4EBP1, and eIF4E translation initiating factor. It is known that activation of ERK induces the phosphorylation of eIF4E by the MNK kinase (31) and of 4EBP1 by inactivation of TSC2 through p90RSK (32). In turn, phosphorylation of 4EBP1 releases eIF4E, thus allowing protein translation. We found that PLX4720 turns off the MAPK pathway in $BRAF^{V600E}$ mutated cells, resulting in decreased phosphorylation of p90RSK1, 4EBP1, and eIF4E. The same effect could not be recapitulated in DiFi cancer cells, demonstrating that it is dependent on the presence of oncogenic BRAF (Fig. 6*C*). Overall, these results indicate that $BRAF^{V600E}$ targeted by PLX4720 modifies the proangiogenic program by acting on the MAPK pathway.

Discussion

To support the exponential growth of solid tumors, new blood vessels are continuously formed (1, 2). This active process is mainly sustained by cancer cells that produce and release angiogenic factors into the microenvironment, thus promoting neoangiogenesis. Antiangiogenic therapies have been developed to target this course of action, which is primarily driven by soluble growth factors such as VEGF (33, 34).

Therapies aimed at interfering with the tumor microenvironment and those that directly target cancer cells are often considered to represent two independent approaches. This discrepancy occurs despite the fact that the epithelial and stromal compartments are clearly linked at the structural and functional levels. How activation of a given oncogene in epithelial cells modulates the angiogenic response of the surrounding stromal cells is largely unknown. We and others have shown that the mutational profile of individual tumors affect their response to targeted therapies (35, 36). For example, EGFR kinase inhibitors are mainly active in lung cancer cells carrying mutations in the receptor (37, 38); likewise, the occurrence of KRAS mutations impairs the efficacy of anti-EGFR monoclonal antibodies in colorectal cancer (39–41). These findings are helping clinicians to match patients with appropriate drugs, a process often referred to as personalized medicine. Clinical evidence indicates that antiangiogenic therapies are also mainly effective in distinct patient subpopulations, although the molecular bases for this are still unknown (42–44). It is therefore tempting to speculate that the genetic milieu of the epithelial compartment dictates an individual's response to antiangiogenic therapies by modulating the tumor microenvironment.

In this work, we explored the possibility that the mutational activation of an individual oncogene affects the angiogenic potential of cancer cells. As a model, we chose $BRAF^{V600E}$, one of the most aggressive oncogenes frequently detected in colorectal tumors and melanomas (10, 12). We took advantage of a KI model, in which BRAF mutation has been introduced into the genome of non-transformed epithelial cells, hence closely recapitulating the situation observed in human neoplasms (30). This strategy overcomes the limitations of previous studies in which expression of cancer alleles was driven by viral promoters, resulting in expression levels many fold greater than in an endogenous setting. We report that BRAF mutant cells display up-regulation of proangiogenic factors and actively recruited the endothelium. In tumor cells, blockage of $BRAF^{V600E}$ with the specific PLX4720 inhibitor not only exerted a cytostatic activity, but influenced the architecture of tumor vasculature. Notably, PLX4720 treatment did not affect ECs directly; rather, it down-regulated the expression of angiogenic factors in tumor cells by switching off the MAPK pathway and p90RSK-dependent translation.

Treatment with PLX4720 strongly influenced the morphology of the tumor vasculature in the cellular models (COLO205 and SK-MEL-28) that were analyzed. Specifically, the BRAF inhibitor modified the architecture and the functionality of the vessels, which appeared more regularly shaped, and provided a better perfusion of the tumor. Furthermore, in both COLO205 and SK-MEL-28, PLX4720 reduced necrosis and almost completely abrogated tumor hypoxia. We propose that, in addition to the well established growth inhibitory activities on BRAF mutant cancer cells, PLX4720 affects tumor growth by stabilizing the vasculature and ameliorating tissue perfusion. At least in the experimental conditions we tested, $BRAF^{V600E}$ targeting by PLX4720 showed some advantageous features compared with the classical anti-angiogenic therapy with bevacizumab. The latter clearly reduced tumor growth and angiogenesis but did not improve oxygenation or reduce hypoxia. These results are reminiscent of data obtained in mouse models of pancreatic neuroendocrine

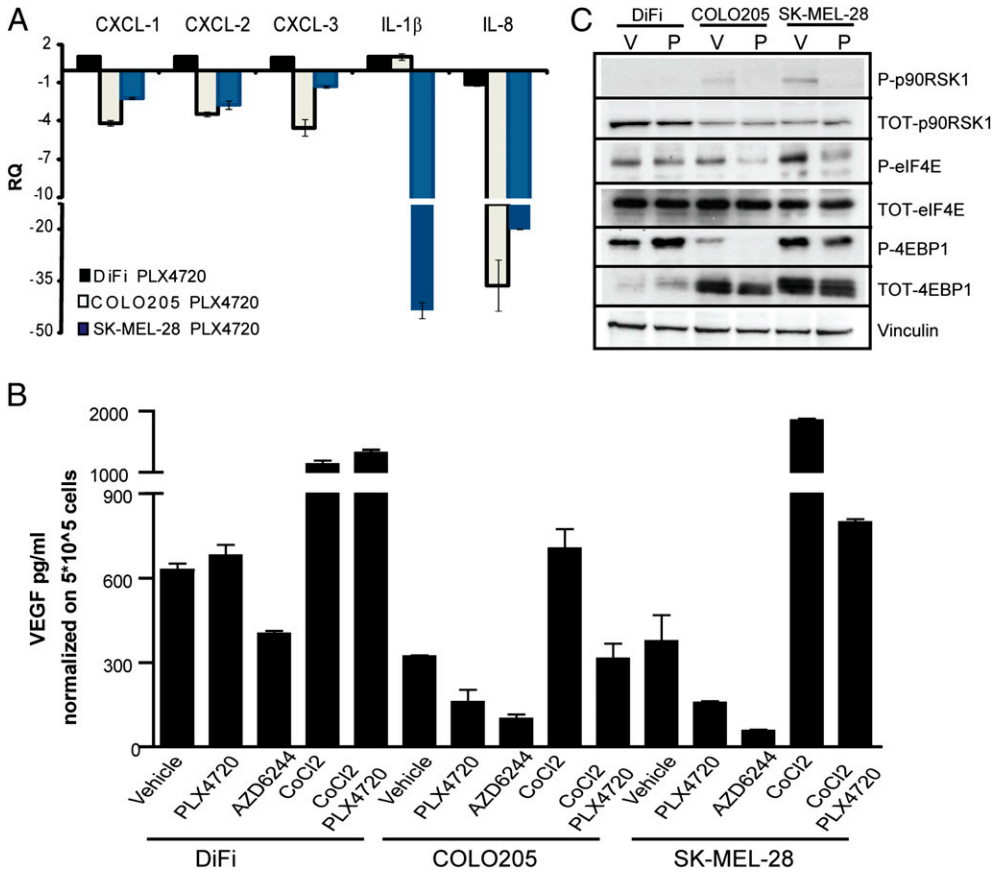

Fig. 6. PLX4720 treatment down-regulates the expression of proangiogenic factors. (*A*) Expression of proangiogenic factors was evaluated by real-time PCR. Cells carrying $BRAF^{V600E}$, COLO205, and SK-MEL-28, and BRAF WT DiFi cells were treated for 24 h with PLX4720. Data are expressed as relative quantity (RQ) of PLX4720 compared with vehicle-treated samples. Bars show mean ± SD of triplicate measurements. (*B*) Quantification of secreted VEGF-A in cells supernatant by ELISA after 24 h of the indicated treatments. Data are expressed in pg/mL and bars represent mean ± SEM of duplicate observations. The representative of two experiments is shown. (*C*) Biochemical analysis of phospho-p90RSK1, -eIF4E, and -4EBP1 in COLO205, SK-MEL-28, and DiFi cells. Protein loading was normalized by vinculin. Starved cells were stimulated for 30 min with 2.5% FBS plus 1 μM PLX4720 or vehicle.

tumor and glioblastoma, whereby compounds that inhibit VEGF receptor 2 induce a marked hypoxia (45, 46).

Although the overall effect of BRAF inhibition was consistent in the two cell types, treatment of SK-MEL-28 reduced the vascularized area whereas the opposite occurred when COLO205 tumors were treated. A number of explanations could account for this difference. It has been reported that the ratio of the VEGF-A isoforms dictates the final shape of the vasculature and regulates blood flow by influencing vessel size (47, 48). It is possible that the VEGF isoforms and other cytokines are modulated to different extents in the two models. Moreover, VEGF activities may be finely tuned by specific coreceptors of VEGF-receptor 2 (e.g., neuropilins, integrins) that may be differentially expressed on the capillaries of the two xenografts (49). Finally, the effect of PLX4720 on SK-MEL-28 tumor vasculature is in line with the phenotype observed by treating melanoma tumors with VEGF-receptor inhibitor. As a matter of fact, in the SK-MEL-3 melanoma model, treatment with sunitinib caused a significantly decrease in vessel density, but the pressure of oxygen and uptake of contrast agent used in resonance imaging were increased (50).

The efficacy and safety of antiangiogenic agents has recently been questioned based on the discovery that reducing the blood supply to cancer cells causes hypoxia and could favor metastasization (45, 46, 51). In this regard, our work suggests that the pharmacological inhibition of an oncogenic mutation, which causally contributes to the imbalance between pro- and antiangiogenic mediators, may represent another valuable strategy to target tumor angiogenesis.

Materials and Methods

Isogenic Cell Model. hTERT-HME1 cells were purchased from American Type Culture Collection, and KI cells for $BRAF^{V600E}$ were obtained through adenoassociated viral-mediated homologous recombination as previously described (30).

CAM Assay. Fertilized chicken embryos were incubated for 3 d at 37 °C and 70% humidity. A small hole was made over the air sac at the end of the egg, and a second hole was made directly over the embryonic CAM. After 10 d, hTERT-HME1 WT or $BRAF^{V600E}$ KI cells were inoculated onto CAM for 48 h. In detail, 1×10^6 cells were mixed with 50 μL of serum-free DMEM plus 50 μL of Matrigel (growth factors reduced; Becton-Dickinson) and dropped onto the CAM to form a plug. CAMs were fixed with PBS solution/3.7% paraformaldehyde for 10 min at room temperature, and images were taken with a QIcam FAST1394 digital color camera (QImaging) connected to the stereomicroscope (model SZX9;Olympus). *SI Materials and Methods* describes the quantification of CAM vasculature.

Mouse Xenografts. All animal procedures were approved by the ethical commission of the University of Turin and the Italian Ministry of Health. COLO205 (5×10^6 cells per mouse) or SK-MEL-28 (8×10^6 cells per mouse) were injected s.c. into the right posterior flanks of 7-wk-old immunodeficient NOD/SCID female mice (6 mice per group; Charles River). Tumor formation was monitored twice per week, and tumor volume based on caliper measurements was calculated by the modified ellipsoid formula (i.e., half the product of length and the square of width). When tumors reached a volume of approximately 150 to 200 mm^3, mice were randomized and treated by daily gavage for 2 wk with vehicle (1% methylcellulose, 5% DMSO in sterile water) or PLX4720 60 mg/kg.

Hypoxia Assay. Tumor hypoxia was detected by the formation of pimonidazole adducts with a Hypoxyprobe-1 Plus (FITC-mAb) kit (HP2-200; HPI) following manufacturer instructions. Details about the procedure and quantification are provided in *SI Materials and Methods*.

Tumor Vasculature Quantification. The following primary antibodies were used for histological analysis: rabbit anti-von Willebrand Factor (vWF; A0082; DakoCytomation), mouse anti–HLA-ABC antigen (M0736; DakoCytomation), rabbit anti-Ki67 (RM-9106-F0; Thermo Scientific) rat anti-CD31 (Pecam-1; 550274BD; Pharmingen), anti-NG2 (chondroitin sulfate proteoglycan polyclonal; AB5320; Chemicon). Quantifications on tumor vasculature were performed with Image-Pro Plus 6.2 software (Media Cybernetics). The surface area occupied by vessels was quantified as surface area of anti-CD31 antibody staining compared with total tissue area visualized by DAPI. For each animal, the total vessel area of at least four field/images was quantified.

Quantification of blood vessel lumen diameter was performed on single stack images with Image-Pro Plus 6.2 software (Media Cybernetics). This analysis was performed with the same images used for determination of surface area occupied by vessels.

ACKNOWLEDGMENTS. We thank Famarco and Susa Trasporti for providing white Leghorn chicken eggs; Dr. G. Serini, Dr. Paolo Michieli, Dr. Enrico Giraudo, Dr. Serena Marchiò, and Dr. Emily Crowley for criticisms and suggestions; and Dr. Sebastjian Hobor and Dr. Sandra Misale for help with mouse handling and ELISA experiments. Work in the laboratories of the authors is supported by the Italian Association for Cancer Research (A. Bardelli and F.B.); the Italian Ministry of Health, Ricerca Oncologica-PIO 2006 (to A. Bardelli); Ricerca Finalizzata 2006 (F.B.); Fondo per gli Investimenti della Ricerca di Base Grant RBAP11BYNP (to F.B.); Nanosistemi avanzati per una nuova oncologia molecolare (NEWTON) (F.B.); Regione Piemonte, Ricerca Finalizzata 2008–2009 (A. Bardelli, F.D.N., and F.B.); Ricerca Industriale e Competitiva 2006; Ricerca Tecnologie Convergenti 2007; Grant Photonic Biosensors for Early Cancer Diagnostics; Piattaforme Tecnologiche per le Biotecnologie Grant Druidi (Drug Innovation and Discovery); the Italian Ministry of University and Research (A. Bardelli and F.B.). The research leading to these results has received funding from the European Community's Seventh Framework Programme under grant agreement n. 259015 COLTHERES (to A. Bardelli) and grant agreement n. 218071 CANCERGENE (to A. Bardelli); Associazione Italiana per la Ricerca sul Cancro (AIRC)–2010 Special Program Molecular Clinical Oncology 5xMille, project 9970 (to A. Bardelli and F.B.); Fondazione CRT-Torino (F.B.); and Intramural Grant "5 × mille" 2008 Fondazione Piemontese per la Ricerca sul Cancro ONLUS (to A. Bardelli and F.D.N.).

1. Hanahan D, Folkman J (1996) Patterns and emerging mechanisms of the angiogenic switch during tumorigenesis. *Cell* 86:353–364.
2. Bergers G, Benjamin LE (2003) Tumorigenesis and the angiogenic switch. *Nat Rev Cancer* 3:401–410.
3. Jain RK (2005) Normalization of tumor vasculature: An emerging concept in antiangiogenic therapy. *Science* 307:58–62.
4. Bottaro DP, Liotta LA (2003) Cancer: Out of air is not out of action. *Nature* 423: 593–595.
5. Vaupel P, Kelleher DK, Höckel M (2001) Oxygen status of malignant tumors: pathogenesis of hypoxia and significance for tumor therapy. *Semin Oncol* 28(2 suppl 8)29–35.
6. Rak J, Yu JL, Kerbel RS, Coomber BL (2002) What do oncogenic mutations have to do with angiogenesis/vascular dependence of tumors? *Cancer Res* 62:1931–1934.
7. Rak J, et al. (1995) Mutant ras oncogenes upregulate VEGF/VPF expression: Implications for induction and inhibition of tumor angiogenesis. *Cancer Res* 55:4575–4580.
8. Okada F, et al. (1998) Impact of oncogenes in tumor angiogenesis: Mutant K-ras upregulation of vascular endothelial growth factor/vascular permeability factor is necessary, but not sufficient for tumorigenicity of human colorectal carcinoma cells. *Proc Natl Acad Sci USA* 95:3609–3614.
9. Sparmann A, Bar-Sagi D (2004) Ras-induced interleukin-8 expression plays a critical role in tumor growth and angiogenesis. *Cancer Cell* 6:447–458.
10. Davies H, et al. (2002) Mutations of the BRAF gene in human cancer. *Nature* 417: 949–954.
11. Wan PT, et al.; Cancer Genome Project (2004) Mechanism of activation of the RAF-ERK signaling pathway by oncogenic mutations of B-RAF. *Cell* 116:855–867.
12. Garnett MJ, Marais R (2004) Guilty as charged: B-RAF is a human oncogene. *Cancer Cell* 6:313–319.
13. Sartore-Bianchi A, et al. (2009) Multi-determinants analysis of molecular alterations for predicting clinical benefit to EGFR-targeted monoclonal antibodies in colorectal cancer. *PLoS ONE* 4:e7287.
14. Souglakos J, et al. (2009) Prognostic and predictive value of common mutations for treatment response and survival in patients with metastatic colorectal cancer. *Br J Cancer* 101:465–472.
15. Xing M, et al. (2005) BRAF mutation predicts a poorer clinical prognosis for papillary thyroid cancer. *J Clin Endocrinol Metab* 90:6373–6379.
16. Xing M (2010) Prognostic utility of BRAF mutation in papillary thyroid cancer. *Mol Cell Endocrinol* 321:86–93.
17. Tol J, Nagtegaal ID, Punt CJ (2009) BRAF mutation in metastatic colorectal cancer. *N Engl J Med* 361:98–99.
18. Sumimoto H, Imabayashi F, Iwata T, Kawakami Y (2006) The BRAF-MAPK signaling pathway is essential for cancer-immune evasion in human melanoma cells. *J Exp Med* 203:1651–1656.
19. Mesa C, Jr., et al. (2006) Conditional activation of RET/PTC3 and BRAFV600E in thyroid cells is associated with gene expression profiles that predict a preferential role of BRAF in extracellular matrix remodeling. *Cancer Res* 66:6521–6529.
20. Kumar SM, et al. (2007) Mutant V600E BRAF increases hypoxia inducible factor-1alpha expression in melanoma. *Cancer Res* 67:3177–3184.
21. Zerilli M, et al. (2010) BRAF(V600E) mutation influences hypoxia-inducible factor-1alpha expression levels in papillary thyroid cancer. *Mod Pathol* 23:1052–1060.
22. Kikuchi H, Pino MS, Zeng M, Shirasawa S, Chung DC (2009) Oncogenic KRAS and BRAF differentially regulate hypoxia-inducible factor-1alpha and -2alpha in colon cancer. *Cancer Res* 69:8499–8506.
23. Sharma A, et al. (2005) Mutant V599EB-Raf regulates growth and vascular development of malignant melanoma tumors. *Cancer Res* 65:2412–2421.
24. Liang S, Sharma A, Peng HH, Robertson G, Dong C (2007) Targeting mutant (V600E) B-Raf in melanoma interrupts immunoediting of leukocyte functions and melanoma extravasation. *Cancer Res* 67:5814–5820.
25. Niault TS, Baccarini M (2010) Targets of Raf in tumorigenesis. *Carcinogenesis* 31: 1165–1174.
26. Nucera C, et al. (2010) B-Raf(V600E) and thrombospondin-1 promote thyroid cancer progression. *Proc Natl Acad Sci USA* 107:10649–10654.
27. Bollag G, et al. (2010) Clinical efficacy of a RAF inhibitor needs broad target blockade in BRAF-mutant melanoma. *Nature* 467:596–599.
28. Flaherty KT, et al. (2010) Inhibition of mutated, activated BRAF in metastatic melanoma. *N Engl J Med* 363:809–819.
29. Chapman PB, et al.; BRIM-3 Study Group (2011) Improved survival with vemurafenib in melanoma with BRAF V600E mutation. *N Engl J Med* 364:2507–2516.
30. Di Nicolantonio F, et al. (2008) Replacement of normal with mutant alleles in the genome of normal human cells unveils mutation-specific drug responses. *Proc Natl Acad Sci USA* 105:20864–20869.
31. Ueda T, Watanabe-Fukunaga R, Fukuyama H, Nagata S, Fukunaga R (2004) Mnk2 and Mnk1 are essential for constitutive and inducible phosphorylation of eukaryotic initiation factor 4E but not for cell growth or development. *Mol Cell Biol* 24:6539–6549.
32. Roux PP, Ballif BA, Anjum R, Gygi SP, Blenis J (2004) Tumor-promoting phorbol esters and activated Ras inactivate the tuberous sclerosis tumor suppressor complex via p90 ribosomal S6 kinase. *Proc Natl Acad Sci USA* 101:13489–13494.
33. Ferrara N, Mass RD, Campa C, Kim R (2007) Targeting VEGF-A to treat cancer and age-related macular degeneration. *Annu Rev Med* 58:491–504.
34. Ferrara N, Kerbel RS (2005) Angiogenesis as a therapeutic target. *Nature* 438:967–974.
35. Bardelli A, Siena S (2010) Molecular mechanisms of resistance to cetuximab and panitumumab in colorectal cancer. *J Clin Oncol* 28:1254–1261.
36. Normanno N, et al. (2009) Implications for KRAS status and EGFR-targeted therapies in metastatic CRC. *Nat Rev Clin Oncol* 6:519–527.
37. Lynch TJ, et al. (2004) Activating mutations in the epidermal growth factor receptor underlying responsiveness of non-small-cell lung cancer to gefitinib. *N Engl J Med* 350:2129–2139.
38. Paez JG, et al. (2004) EGFR mutations in lung cancer: Correlation with clinical response to gefitinib therapy. *Science* 304:1497–1500.
39. Lièvre A, et al. (2006) KRAS mutation status is predictive of response to cetuximab therapy in colorectal cancer. *Cancer Res* 66:3992–3995.
40. Benvenuti S, et al. (2007) Oncogenic activation of the RAS/RAF signaling pathway impairs the response of metastatic colorectal cancers to anti-epidermal growth factor receptor antibody therapies. *Cancer Res* 67:2643–2648.
41. Karapetis CS, et al. (2008) K-ras mutations and benefit from cetuximab in advanced colorectal cancer. *N Engl J Med* 359:1757–1765.
42. Kabbinavar FF, et al. (2005) Addition of bevacizumab to bolus fluorouracil and leucovorin in first-line metastatic colorectal cancer: Results of a randomized phase II trial. *J Clin Oncol* 23:3697–3705.
43. Johnson DH, et al. (2004) Randomized phase II trial comparing bevacizumab plus carboplatin and paclitaxel with carboplatin and paclitaxel alone in previously untreated locally advanced or metastatic non-small-cell lung cancer. *J Clin Oncol* 22:2184–2191.
44. Burger RA, Sill MW, Monk BJ, Greer BE, Sorosky JI (2007) Phase II trial of bevacizumab in persistent or recurrent epithelial ovarian cancer or primary peritoneal cancer: A Gynecologic Oncology Group Study. *J Clin Oncol* 25:5165–5171.
45. Pàez-Ribes M, et al. (2009) Antiangiogenic therapy elicits malignant progression of tumors to increased local invasion and distant metastasis. *Cancer Cell* 15:220–231.
46. Ebos JM, et al. (2009) Accelerated metastasis after short-term treatment with a potent inhibitor of tumor angiogenesis. *Cancer Cell* 15:232–239.
47. Lee S, Jilani SM, Nikolova GV, Carpizo D, Iruela-Arispe ML (2005) Processing of VEGF-A by matrix metalloproteinases regulates bioavailability and vascular patterning in tumors. *J Cell Biol* 169:681–691.
48. Gerhardt H, et al. (2003) VEGF guides angiogenic sprouting utilizing endothelial tip cell filopodia. *J Cell Biol* 161:1163–1177.
49. Ferrara N, Gerber HP, LeCouter J (2003) The biology of VEGF and its receptors. *Nat Med* 9:669–676.
50. Eichhorn ME, et al. (2008) Contrast enhanced MRI and intravital fluorescence microscopy indicate improved tumor microcirculation in highly vascularized melanomas upon short-term anti-VEGFR treatment. *Cancer Biol Ther* 7:1006–1013.
51. Chan DA, Giaccia AJ (2007) Hypoxia, gene expression, and metastasis. *Cancer Metastasis Rev* 26:333–339.

Supporting Information

Bottos et al. 10.1073/pnas.1105026109

SI Materials and Methods

Cell Culture. hTERT-HME1 cells were purchased from American Type Culture Collection and were cultured in growth medium containing DMEM/F-12 (Invitrogen) supplemented with 20 ng/mL EGF, 10 μg/mL insulin, and 100 μg/mL hydrocortisone. COLO205 and SK-MEL-28 cell lines were purchased from American Type Culture Collection and cultured in RPMI-1640 medium (Invitrogen). DiFi cells were supplied by José Baselga (Vall d'Hebron University, Barcelona, Spain) and cultured in Ham F-12 medium (Clonetics/Cambrex Bio Science). All cell media were supplemented with 10% FBS (Gibco/Invitrogen), penicillin (500 U/mL), and streptomycin (100 μg/mL). Human endothelial cells (ECs) were isolated from umbilical cord vein, characterized, and grown as previously described (1).

Quantification of Chicken Chorioallantoic Membrane Vasculature. For each chicken chorioallantoic membrane (CAM) sample, an arbitrary "angiogenic index" was scored on the basis of microvessel density and/or hemorrhages. Three categories were defined: "low" index when microvessels or hemorrhages were absent, "medium" when present in 30% to 70% of the surface area, or "high" when occupying almost the complete area of the plug.

For histological analysis, samples were fixed in Zin-fixative and frozen in cryostat embedding medium (Killik; Bio-Optica) to prepare sections. Chicken ECs were visualized by the endothelial marker von-Willebrand Factor and human epithelial cells by HLA antigen (as detailed later). Single stack images were acquired by confocal laser-scanning microscope (TCS SP2 with DM IRE2; Leica) equipped with 20×, 40×, and 63×/1.40 HCX plan-apochromat oil-immersion objective.

Quantification of ECs recruitment by hTERT-HME1 cell was performed by Leica Confocal Software Histogram Quantification Tool. In each picture, we drew a region of interest following anti-HLA staining that recognized hTERT-HME1, and we quantified the mean fluorescence intensity of anti-von Willebrand Factor staining in the same area. Three images for each sample were analyzed and the results are expressed as mean ± SEM of individual CAM.

Real-Time PCR. The total RNA was extracted from cell cultures or fresh chorioallantoic membrane tissues by using the phenol-chloroform method (Trizma; Sigma-Aldrich), treated with DNase-free kit (Ambion; Applied Biosystems), and quantified with an RNA 6000 Nano Assay kit in an Agilent 2100 Bioanalyzer (Agilent Technologies). Single-strand cDNA synthesis from total RNA was prepared by TaqMan reverse transcription reagents (Applied Biosystems), as recommended by the manufacturer. All quantitative real-time PCR reactions were performed with ABI PRISM 7900 HT Fast Real-Time PCR system (Applied Biosystems). The expression of the housekeeping gene, TATA Binding Protein (TBP), was used to normalize for variances in input cDNA. All measurements were performed in technical duplicates. Raw data were analyzed using SDS2.2 software (Applied Biosystems) to define relative quantity (RQ) and the gene expression data analysis program GEDAS (http://sourceforge.net/projects/gedas) for hierarchical clustering.

The following TaqMan Gene Expression Assay (Applied Biosystems) has been used for the analysis: ADAMTS1-Hs00199608_m1, ADM-Hs00181605_m1:00 AMOT-Hs00611096_m1, ANGPT1-Hs00181613_m1, CCL2-Hs00234140_m1, CD44-Hs00153304_m1, COL15A1-Hs01559630_m1, COL4A1-Hs01007469_m1, CSF1-Hs00174164_m1, CSF3-Hs99999083_m1, CTGF-Hs00170014_m1, CXCL12-Hs00171022_m1, CXCL1-Hs00605382_gH, CXCL2-Hs00601975_m1, CXCL3-Hs00171061_m1, CYR61-Hs00155479_m1, EDG1-Hs01922614_s1, EDIL3-Hs00174781_m1, EGR1-Hs00152928_m1, EPAS1-Hs01026142_m1, EPHB2-Hs00362096_m1, FAS-Hs00163653_m1, FBLN5-Hs00197064_m1, FST-Hs00246256_m1, HEY1-Hs00232618_m1, HGF-Hs00300159_m1, HSPG2-Hs01078536_m1, ICAM1-Hs00164932_m1, IGF2-Hs00171254_m1, IL1B-Hs00174097_m1, IL11-Hs00174148_m1, IL12A-Hs00168405_m1, IL6-Hs00174131_m1, IL8-Hs00174103_m1, ITGA4-Hs00168433_m1, ITGAV-Hs00233808_m1, ITGB2-Hs00164957_m1, KDR-Hs00176676_m1, MDK-Hs00171064_m1, MMP2-Hs00234422_m1, MMP3-Hs00968308_m1, MMP9-Hs00234579_m1, PDGFB-Hs00234042_m1, PDGFRA-Hs00998026_m1, PDGFRB-Hs00387364_m1, PECAM1-Hs00169777_m1, PTGS2-Hs00153133_m1, PTN-Hs00383235_m1, SEMA3A-Hs00173810_m1, SERPINB5-Hs00184728_m1, SERPINF1-Hs00171467_m1, SLIT2-Hs00191193_m1, TGFA-Hs00608187_m1, TGFB2-Hs00234244_m1, TGFBR2-Hs00559661_m1, TNF-Hs00174128_m1, VEGFC-Hs00153458_m1, VEGF-Hs00900054_m1.

EC Migration. Chemotaxis assays with human ECs were performed with a Boyden chamber, which consists of a 48-well microchemotaxis chamber (Neuroprobe) and polyvinylpyrrolidone-free polycarbonate filters (Nucleopore; Corning Costar) with a pore size of 8 μm coated with 1% gelatin. hTERT-HME1 WT or $BRAF^{V600E}$ knock-in (KI; 1×10^6) were cultured for 36 h in serum-free DMEM, and then supernatants were collected and added in the lower compartment of the Boyden chamber. Rabbit anti–hVEGF-A (500-P10; PeproTech) blocking antibody 10 μg/mL, or unrelated immunoglobulins (X0903; DakoCytomation) were added to cell supernatants. ECs cells were serum-starved overnight, and 50 μL of 2.5×10^6 cells/mL suspension were added to the upper compartment in serum-free medium. To test the effect of PLX4720 on endothelium, ECs were treated for 24 h with 1 μM PLX4720 in starved condition and then stimulated with complete medium or VEGF-A (R&D Systems) for migration. After 5 h of incubation at 37 °C with 5% CO_2, the upper surface of the filters was scraped with a rubber policeman scraper, and the filters were fixed and stained with Diff-Quick (Dade Behring). Four random fields of each sample in the lower surface of the filters were counted at a magnification of 10× with a BX-60 microscope (Olympus) equipped with a color Qicam Fast 1394-digital CCD camera (12 bit; QImaging). All samples were analyzed in triplicate and data are expressed as mean ± SD.

ELISA. Parental or $BRAF^{V600E}$ hTERT-HME1 (7×10^5) were cultured for 24 h in serum-free DMEM. COLO205, SK-MEL-28, and DiFi cells (5×10^5) were plated in six-well dishes and treated for 24 h with 1 μM PLX4720, $CoCl_2$ 100 μM, the MEK inhibitor AZD6244 100 nM, or vehicle in RPMI 1% serum. Supernatants were collected and cells were counted to normalized VEGF-A quantification on the total number of cells.

ELISA for VEGF-A was performed with a Quantikine immunoassay kit (DVE00; R&D Systems) following the manufacturer's instructions.

PLX4720 Synthesis. PLX4720 was provided by Alberto Minassi and Giovanni Appendino (Universitá del Piemonte Orientale, Novara, Italy) and synthesized as previously described (2).

Hypoxia Assay. Tumor hypoxia was detected by the formation of pimonidazole adducts with Hypoxyprobe-1 Plus (FITC-mAb) kit

(HP2-200; HPI) and following manufacturer instructions. Briefly, mice were injected intraperitoneally with pimonidazole hydrochloride and euthanized after 90 min. Tumors were frozen in cryostat embedding medium (Killik; Bio-Optica) for histological analysis. The percentage hypoxic surface area was quantified using Image-Pro Plus 6.2 software (Media Cybernetics) by measuring pimonidazole-stained area compared with the total tissues area. For each mouse, the hypoxic area was defined by the sum of at least three fields at a magnification of 5× with an BX-60 microscope (Olympus) equipped with a color Qicam Fast 1394-digital CCD camera (12 bit; QImaging). Individual animals were used to calculate mean and SEM.

Tissue Perfusion. Blood vessel perfusion was detected by i.v. administration of 200 μL of orange fluorescent microspheres (FluoSpheres; Molecular Probes). After 2 min, the animals were killed and tumor tissues were fixed by heart perfusion with ice-cold PFA 2% (wt/vol). The distribution of the microspheres in tumors was visualized by confocal microscopy by using 10-μm sections. Tumor perfusion was quantified as colocalization signal between microspheres and blood vessels on multiple stacks images with LAS AF software (Leica) maintaining the same area (0.303 mm^2) and fluorescent setting. At least 10 images at a magnification of 40× were analyzed for each sample, with five mice per treatment group.

Histological Analysis. Tumor tissues were fixed by heart perfusion with ice-cold PFA 2% (wt/vol). Tissue slides (12 μm) were treated following standard immunofluorescence or immunohistochemistry procedures. Briefly, slides were permeabilized in 0.2% Triton X-100 (Sigma-Aldrich), treated for 5 to 20 min with 3% hydrogen peroxide (Sigma-Aldrich) to quench endogenous peroxidases in immunohistochemistry experiments, and saturated in 3% BSA (wt/vol; Sigma-Aldrich).

For immunohistochemistry, secondary HRP-conjugate antibodies (EnVision; DakoCytomation) were used, and the reaction was visualized with the AEC kit (DakoCytomation). When necessary, tissues were counterstained with Mayer hematoxylin (Vector Laboratories), mounted on glass slides, and visualized with a BX-60 microscope (Olympus) equipped with a color Qicam Fast 1394-digital CCD camera (12 bit; QImaging).

For immunofluorescence experiments, Alexa Fluor secondary antibodies (Invitrogen) were used. Tissues were counterstained with DAPI nucleic acid stain (Invitrogen), and analyses were performed by using a Leica TCS SP2 AOBS confocal laser-scanning microscope (Leica Microsystems).

Blood vessels coverage by pericytes was defined by the measure of colocalization area between anti-CD31 and anti-NG2 staining with Image-Pro Plus 6.2 software (Media Cybernetics). Final results were normalized on total area occupied by vessels.

Proliferation Assay. COLO205, SK-MEL-28, and DiFi cells (2.5×10^3) were seeded in quadruplicate in 96-well plates in complete medium. After 24 h, cells were treated for 96 h with increasing concentrations of PLX4720 in RPMI 5% serum. ECs (2×10^3) were seeded in starved condition and stimulated with serum or VEGF-A (R&D Systems) with 1 μM PLX4720 or vehicle for 96 h. Cell viability was evaluated by a luminescence ATP assay (Cell-Titer Glo; Promega). All luminescence were recorded by the DTX 880-Multimode plate reader (Beckman-Coulter).

Western Blotting. Total protein lysates from tumor cells or xenografts were obtained by warm Laemmli buffer extraction (SDS 5%, Tris-HCl 0.15 M, pH 6.8, 4% glycerol). Cell lysates (30 μg) were separated by SDS/PAGE electrophoresis and transferred to nitrocellulose membrane (Hybond-C Extra; Amersham Biosciences). After blocking with 10% BSA, membranes were incubated with primary antibodies overnight at 4 °C. The following antibodies were used: mouse anti–phospho-p44/42 MAPK (Erk1/2; Thr202/Tyr204; 9106; Cell Signaling), rabbit anti-p44/42 MAPK (Erk1/2; 9102; Cell Signaling), rabbit anti–phospho-AKT (Ser473; 9271; Cell Signaling), rabbit anti–phospho-AKT (Thr308; 2965; Cell Signaling), rabbit anti-AKT (9272; Cell Signaling), rabbit anti–phospho-eIF4E (Ser209; 9741; Cell Signaling), rabbit anti-eIF4E (9742; Cell Signaling), rabbit anti–phospho-4EBP1 (Ser65; 9451; Cell Signaling), rabbit anti-4EBP1 (9452; Cell Signaling), rabbit anti–phospho-p90RSK (Ser380; 9D9; 9335; Cell Signaling), rabbit anti-p90RSK (9333; Cell Signaling), goat anti-vinculin (*N*-19; sc-7649; Santa Cruz Biotechnology), and rabbit anti–cleaved caspase-3 (Asp175; 9664; Cell Signaling). After incubation with peroxidase-conjugated secondary antibodies (305-035-003, diluted 1:15,000; Jackson ImmmunoResearch), proteins were detected by ECL (Perkin-Elmer).

1. Bussolino F, et al. (1992) Hepatocyte growth factor is a potent angiogenic factor which stimulates endothelial cell motility and growth. *J Cell Biol* 119:629–641.

2. Tsai J, et al. (2008) Discovery of a selective inhibitor of oncogenic B-Raf kinase with potent antimelanoma activity. *Proc Natl Acad Sci USA* 105:3041–3046.

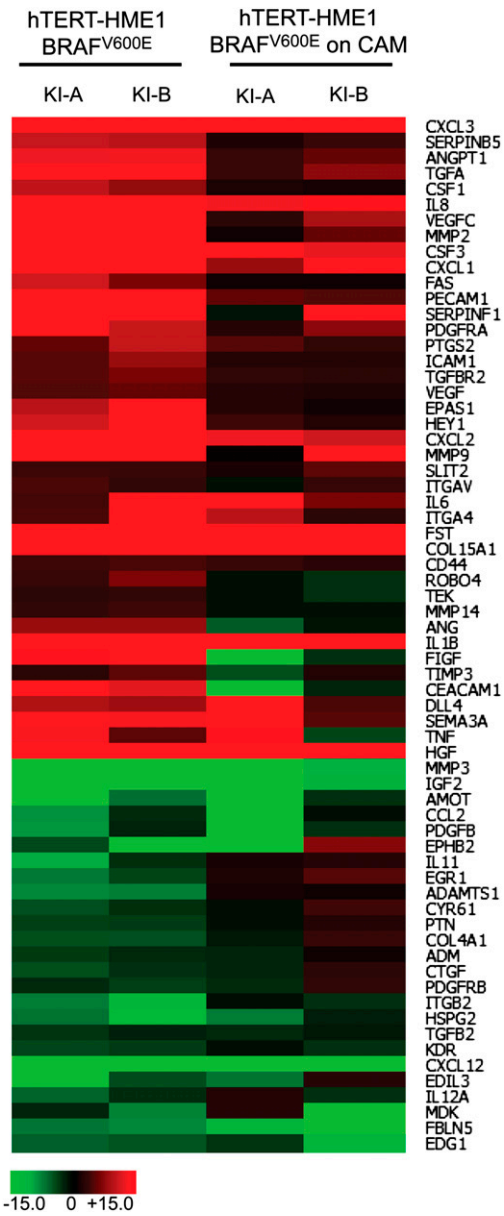

Fig. S1. BRAF^{V600E} up-regulates the expression of proangiogenic factors in hTERT-HME1 BRAF^{V600E} KI cells. Gene expression analysis was performed by real-time PCR comparing parental hTERT-HME1 with two different BRAF^{V600E} clones (KI-A and KI-B). The transcription profile was analyzed in cells plated on culture dish or on CAM. Differentially modulated genes were selected and analyzed by hierarchical clustering. Data are plotted as relative quantity mean on a scale from −15 to +15 fold change.

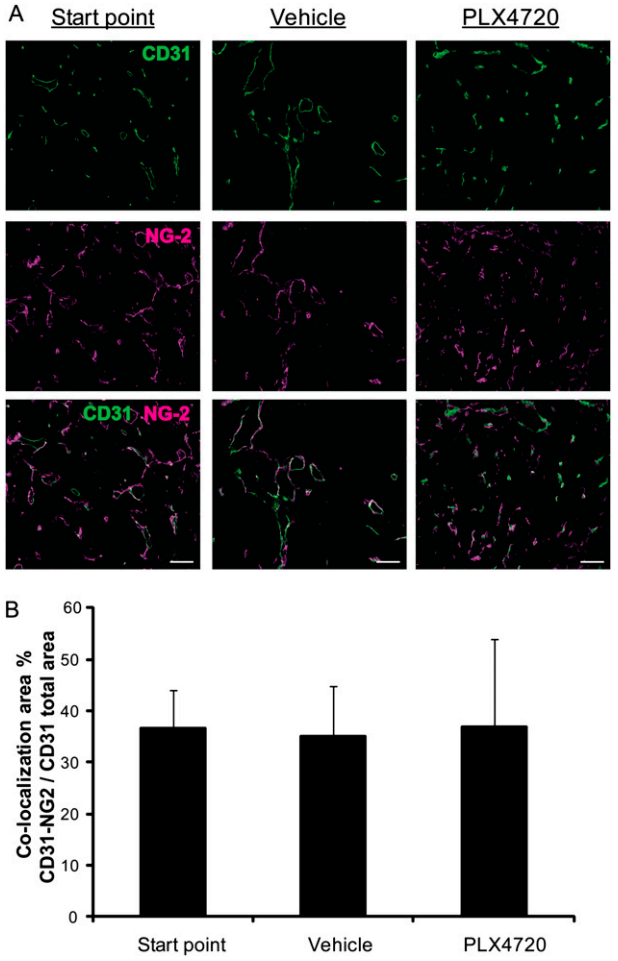

Fig. S2. PLX4720 treatment does not influence blood vessel coverage by pericytes. Histological analysis of COLO205 xenografts before and after PLX4720 treatment. (*A*) Immunofluorescence analysis upon staining with the CD31 endothelial marker (green) and NG-2 pericyte marker (magenta) with colocalization of the two markers. (Scale bar: 100 μm.) (*B*) Percentage areas of colocalization between CD31 and NG-2 stainings. Data are normalized on CD31 surface area. Bars show mean ± SEM. Start point, n = 4 mice; vehicle, n = 6 mice; PLX4720, n = 6 mice.

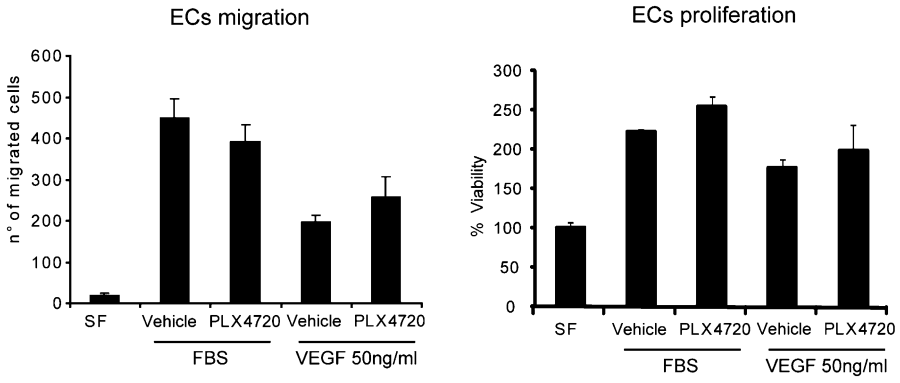

Fig. S3. PLX4720 does not affect ECs proliferation and migration. Human ECs were used to evaluate migration and proliferation. ECs were stimulated by serum (i.e., FBS) or 50 ng/mL VEGF-A and were treated with 1 μM PLX4720 or vehicle. EC migration is represented as mean number of migrated cells ± SD in triplicate. Cells proliferation is shown as mean percentage of cells viability compared with untreated samples (SF) ± SD in quadruplicate. In both cases, representative results of two independent experiments are shown.